3D multilayered Bi4O5Br2 nanoshells displaying excellent visible light photocatalytic degradation behavior for resorcinol

Journal:	*Micro & Nano Letters*
Manuscript ID	MNL-2017-0886.R1
Manuscript Type:	Letter
Date Submitted by the Author:	31-Mar-2018

Complete List of Authors:	Hu, Hanmei; Anhui University of Architecture, School of Materials and Chemical Engineering Xu, Juanjuan; Anhui Jianzhu University South Campus, School of Materials and Chemical Engineering Deng, Chonghai; Hefei University, Department of Chemical and Materials Engineering Wang, Man Zhou, Xiaoyu; Hefei University, Department of Chemical and Materials Engineering Le, Huirong; University of Derby, Department of Mechanical Engineering and Built Environment

Keyword:	CRYSTAL GROWTH, NANOCRYSTALLINE MATERIALS, SCANNING ELECTRON MICROSCOPY, SYNTHESIS, CATALYSTS

3D multilayered $Bi_4O_5Br_2$ nanoshells displaying excellent visible light photocatalytic degradation behavior for resorcinol

*H. M. Hu[1] *, J. J. Xu[1], C. H. Deng[2,3]*, M. Wang[1], X. Y. Zhou[2] and H. R. Le[3]*

[1] *Key Laboratory of Functional Molecule Design and Interface Process, Anhui Jianzhu University, Hefei, 230601, China*
[2] *Department of Chemical and Materials Engineering, Hefei University, Hefei, 230601, China*
[3] *Department of Mechanical Engineering and Built Environment, University of Derby, Derby, England DE22 3AW, United Kingdom*
E-mail: hmhu@ustc.edu (H.M. Hu); chdeng@mail.ustc.edu.cn (C. H. Deng)

High-ordered three-dimensional (3D) multilayered $Bi_4O_5Br_2$ nanoshells have been fabricated successfully via a green ultrasound-assisted anion exchange reaction followed by a calcination treatment approach. The products are characterized by X-ray diffraction (XRD), field-emission scanning electron microscopy (FESEM), transmission electron microscopy (TEM), high resolution transmission electron microscopy (HRTEM), UV-vis diffuse reflectance spectrum (DRS) and N_2 adsorption/desorption isotherms. The results reveal that ternary $Bi_4O_5Br_2$ nanoshells possess a pure monoclinic phase with the average thickness of *ca.* 12 nm, and the walls are of 10-12 layers constructed by nanograins with 10 nm in size. The specific surface is measured to be 36.18 $m^2 \cdot g^{-1}$ and the band gap energy E_g value is calculated to be 2.52 eV. The possible formation process for $Bi_4O_5Br_2$ nanoshells is simply proposed. According to the photocatalytic degradation for resorcinol under visible light irradiation, the as-prepared $Bi_4O_5Br_2$ nanoshells exhibit excellent photocatalytic performance, which is not only far beyond the degradation rate of BiOBr precursor nanosheets, but also superior to that of other reported $Bi_4O_5Br_2$ architectures, suggesting a practical application for the treatment of organic pollutants.

1. Introduction: Nowadays, the increasing demand of energy consumption and the increasing hazard of environmental pollution has significantly affected the health of human beings and hindered the harmonious development of modern society [1-3]. Over decades, the semiconductor-based photocatalysis technology has been considered as a friendly and efficient methodology of environmental remediation and solar fuel conversion [4-7]. As is well known, the semiconductor photocatalysis processes undergo three steps as follows: i, charge electron-hole pairs (e^-/h^+) are generated inside the semiconductor over ultraviolet-visible light irradiation; ii, photo-induced carriers (e^-/h^+) could transport from the inside of the material to the surface; iii, photo-generated carriers (e^-/h^+) may capture the species adsorbed on the surface of the material to cause oxygen/reduction reaction [8-10]. Compared with the bulk, the ultrathin layered semiconductor nanoarchitectures may lead to more exposed interior atoms and induce the formation of various defects, contributing to harvest more solar light and fast transport photo-generation carriers from the inside to the surface, which may significantly increase the photocatalytic activities [11-14].

In recent years, ternary bismuth oxybromide families ($Bi_xO_yBr_z$) have demonstrated excellent photocatalytic application in the field of energy generation and environmental remediation because of unique layered structure, suitable indirect band gap and visible light responsive ability [15-17]. Furthermore, the increasing Bi content in bismuth oxybromide can upshift the conduction band (CB) and valence band (VB) edge, which is beneficial in reducing the band gap energy (E_g) as well as enhancing the visible-light absorption [14]. Among the high-ordered Bi-rich bismuth oxybromide, $Bi_4O_5Br_2$ photocatalyst has attracted particular research interests in the preparation and practical application for the photocatalytic degradation of organic pollutants until very recently. For instance, Li and coworkers synthesized ultrathin $Bi_4O_5Br_2$ nanosheets by an ionic liquids-assisted solvothermal method for the degradation of antibacterial agent ciprofloxacin [14]. Nan et al. fabricated $Bi_4O_5Br_2$ ultrathin nanoflakes by an energy-saving microwave route for selective catalytic oxidation of an industrial organic reaction intermediate benzylalcohol [18]. Yang's group constructed $Bi_4O_5Br_2$ with different morphologies of nanosheets, microspheres and hollow spheres via an ionic liquid-in-water microemulsion procedure for the removal of fungicide o-phenylphenol and antibacterial agent norfloxacin and tetracycline hydrochloride under visible light irradiation [19]. Beyond above, a few types $Bi_4O_5Br_2$ nanoparticles were also produced for the practical application in the photo-degradation of organic contaminants by various of physicochemical methodologies such as a hydrothermal method, a structure reorganization route, a hydrolysis process and an ionic liquid-assisted strategy and so on [20-24]. However, to the best of our knowledge, few publications on the preparation of ultrathin layered $Bi_4O_5Br_2$ nanoshells have been reported in the literature.

Herein, 3D ultrathin layered $Bi_4O_5Br_2$ nanoshells with mesoporous structure have been constructed via a green ultrasound-assisted anion exchange reaction combining an annealing process for the first time. The structure and morphology of product have been characterized in detail. A possible growth mechanism for $Bi_4O_5Br_2$ nanoshells is illustrated briefly. Moreover, excellent photocatalytic performance in the degradation of colorless refractory contaminant resorcinol (RC) over as-prepared sample has also been investigated under visible light irradiation.

2. Experiment: Analytical grade of chemicals were purchased from the Sinopharm Chemical Reagent Company and used as received without any further purification. In the typical procedure, 0.4 mmol $Bi(NO_3)_3 \cdot 5H_2O$ was mixed with 10 mL distilled water in a 100 mL autoclavable bottle and stirred at room temperature. Next, 20 mL cetyltrimethylammonium bromide (CTAB, 0.55 mmol) aqueous solution and 30 mL thiourea ($CS(NH_2)_2$, TU, 10 mmol) aqueous solution were added under stirring continuously. Then the bottle was sealed with attached screw cap and transferred into a sonication bath with the temperature of water bath at 80˚C (KQ-50, 50W). After the ultrasound radiation performing for 30 min and the reaction was cooled naturally to the room temperature, the precipitation was centrifuged and washed with distilled water and absolute ethanol in turn, and then dispersed in ethanol by sonication for 20 min. Subsequently, the suspensoid was drop-coated on a 1×1 cm Si matrix, dried naturally and annealed in air at 480 °C for 2 hour with a rising rate of 3.0 °C·min^{-1}, then the ternary Bi-rich $Bi_4O_5Br_2$ nanoshells were obtained finally.

The phase purity of the as-synthesized products was examined by X-ray diffraction (XRD) using a Bruker D8-advance X-ray diffractometer equipped with Cu Kα radiation (λ = 1.5406 Å). Field-

emission scanning electron microscope (FESEM) images of the sample were taken on a field-emission microscope (FESEM, JEOL JSM-6700F, 15kV). The transmission electron microscope (TEM) and high-resolution transmission electron microscope (HRTEM) images of the samples were performed on a JEOL-2010 transmission electron microscope with an accelerating voltage of 200 kV. N_2 adsorption/desorption isotherms were measured on an automatic surface area and pore analyzer (Tristar II 3020 M). UV-vis diffuse reflectance spectrum (DRS) was recorded on an ultraviolet visible spectrophotometer (Solidspec-3700 DUV).

The evaluation of photocatalytic activity for the as-prepared samples was conducted via photocatalytic degradation of colourless organic pollutant resorcinol ($C_6H_6O_2$, RC) aqueous solution under visible light irradiation at the room temperature. A 300 W Xe arc lamp (CEL-HFX300, Beijing China Education Au-light Co., Ltd) was used as the light source and equipped with an ultraviolet cutoff filter to provide visible light ($\lambda \geqslant 400$ nm). The experiment was performed with photocatalyst (50 mg) suspended in RC aqueous solutions (50 mL, 10 $mg \cdot L^{-1}$) with constant stirring. The suspension was stirred in the dark for 60 min to ensure the adsorption/desorption equilibrium. At the given time intervals, about 4 mL of the suspension was taken for the following analysis after centrifugation. The concentration of RC left in the solution was determined by a UV-Vis spectrophotometer (PerkinElmer Lambda 950).

3. Results and discussion: Fig. 1 displays the typical XRD pattern of the as-resulting product. Quantitative analysis agrees that all diffraction peaks in the diagram is in good agreement with the standard data from JCPDS card no. 37-0699 and is assigned to the pure monoclinic phase $Bi_4O_5Br_2$ with the $P2_1$ space group. The emergence of other impurity phase is not observed. Further, the corresponding crystallite sizes are small based on the obvious broadened reflection peaks. The XRD pattern indicates that the single phase $Bi_4O_5Br_2$ photocatalyst has been prepared successfully.

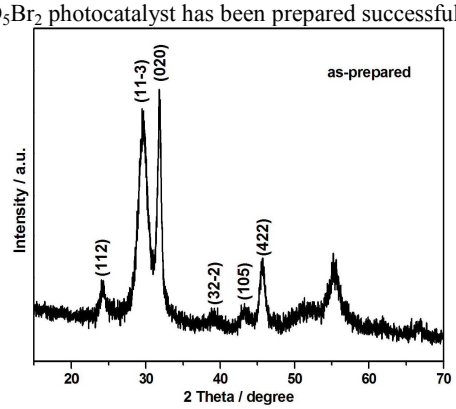

Fig. 1 *XRD pattern of as-resulting $Bi_4O_5Br_2$ sample.*

As given in Fig. 2a, a panoramic FESEM image illustrates that the as-prepared nanoshells appear the 3D quasi hollow structures with the opening diameters ranging from 500 to 800 nm, apart from few irregular nanosheets (indicated by arrows). Some half-spherical architectures (indicated by dotted green circles) show graceful hollow nature. The microstructure of the $Bi_4O_5Br_2$ was further investigated by TEM. As seen in Fig. 2b, a clear contrast between the deeply dark edges and the pale center can be observed, evidently confirming the hollow nanostructure. From the high-magnification TEM image (inset of Fig. 2b), one can see that the walls of an enlarged nanoshell are composed of small nanocrystals with size of about 10 nm, and there are plentiful intercrystal mesopores scattered satellite distribution on the surface. Furthermore, from the side-view high resolution TEM

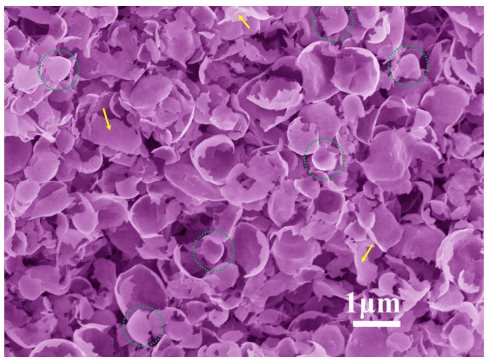

a

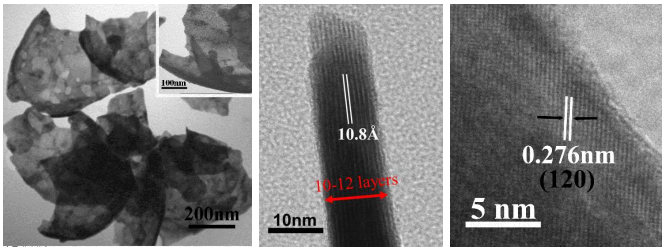

b c d

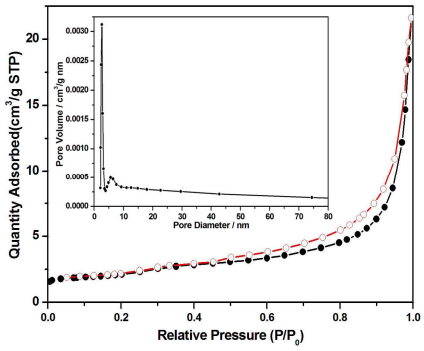

e

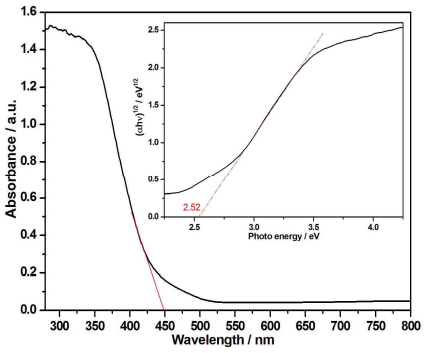

f

Fig. 2 *Characterization of as-prepared sample.*
a FESEM image of shell-like $Bi_4O_5Br_2$ nanostructures
b TEM image of shell-like $Bi_4O_5Br_2$ nanostructures
c Side-view HRTEM image of an individual $Bi_4O_5Br_2$ nanoshell
d Top-view HRTEM image of an individual $Bi_4O_5Br_2$ nanoshell
e N_2 adsorption/desorption isotherms of $Bi_4O_5Br_2$ nanoshells and the pore size distribution (inset)
f UV-vis diffuse reflectance spectrum (DRS) of $Bi_4O_5Br_2$ nanoshells and the estimated E_g value (inset)

(HRTEM) image (Fig. 2c), it can be calculated that the average thickness of shell is *ca.* 11 nm, which is of about 10-12 lattice layers owning of inorganic fullerene-like feature. Besides, according to the top-view HRTEM image (Fig. 2d), the regular lattice fringe spacing of 0.276 nm corresponds to interlayer spacing of the (120) atomic planes of monoclinic $Bi_4O_5Br_2$ [14].

The nitrogen adsorption/desorption isotherms and corresponding pore size distribution curve of the as-obtained 3D $Bi_4O_5Br_2$ nanoshells are displayed in Fig. 2e. The N_2 isotherms exhibits type IV of the Brunauer-Deming-Deming-Teller (BDDT) classification with a type H_3 hysteresis loop, indicating the existence of mesopores. The BET specific surface area of the sample is measured to be 36.2 m^2/g. The inset of pore-size-distribution curve in Fig. 2e shows inhomogeneous mesoporous structure and the multiple pore sizes are estimated to be 2.6 and 5.6 nm in diameter, respectively.

Fig. 2f gives the optical absorption property of the as-synthesized 3D $Bi_4O_5Br_2$ nanoshells, which indicates that the pure $Bi_4O_5Br_2$ has an absorption onset at 450 nm, responding well under visible light. As a crystalline semiconductor, the optical absorption near the band edge follows the formula $\alpha h\nu = A(h\nu-E_g)^{n/2}$ as determined by Kubelka-Munk theory [25], where α, ν, A, and E_g are the absorption coefficient, light frequency, a constant, and band gap energy, respectively. Thus, the E_g of $Bi_4O_5Br_2$ nanoshells can be calculated from the plot of $(\alpha h\nu)^{1/2}$ versus (hν). The intercept of the tangent to the x-axis gives a good approximation of the E_g for $Bi_4O_5Br_2$ nanoshells (inset of Fig. 2f). The estimated Eg value is calculated to be 2.52 eV, which is among the reported results of 2.33~2.54 eV [14, 18, 26].

In our work, two processes including an ultrasonic-assisted anion-exchange reaction and subsequent an *in situ* oxidization reorganization process are applied to yield the $Bi_4O_5Br_2$ nanoarchitectures with ultrathin layered and mesoporous structure. In the present system, $Bi(NO_3)_3$ reacts with water molecule to form slightly soluble $BiONO_3$ sol via an ultrasonic heating firstly [27] [Eq. (1)]. Then, TU, acted as a good complexing reagent, can coordinate with dissociative Bi^{3+} to form $Bi(TU)_n^{3+}$ complexes in order to effectively control the release of Bi^{3+} ions in the solution [28]. While CTAB is introduced in the reaction mixture, due to the rather lower solubility of BiOBr (Ksp 3.0×10^{-7}) relative to $BiONO_3$ (Ksp 2.8×10^{-3}), $BiONO_3$ can transform into BiOBr precipitate based on the anion exchange process [Eq. (2)]. In this procedure, abundant surfactant CTA^+ ions can be adsorbed on the O-terminated (001) surface of BiOBr due to the electrostatic interaction, so the growth of c-axis orientation is inhibited so that the two-dimensional (2D) ultrathin BiOBr precursor nanosheets adsorbing CTAB molecules could be formed [17]. Subsequently, while the 2D ultrathin BiOBr precursor nanosheets are annealed in air atmosphere, due to the curling of 2D nanosheet into 3D nanoshell under the heat treatment accompanied by an *in situ* oxidization reorganization reaction, that is, oxidization causes the crystal structure rearrangement meanwhile heating causes the curling up, the pure 3D ultrathin multilayered and mesoporous $Bi_4O_5Br_2$ nanoshells are finally fabricated [Eq. (3)]. Thus the whole possible schematic diagram can be illustrated in Fig. 3, which is considered to be the sonohydrolysis anion exchange process and following it with the *in situ* oxidization reorganization process. The major chemical reaction is described as follows:

$$Bi^{3+} + NO_3^- + H_2O \leftrightarrow BiONO_3\downarrow + 2H^+ \quad (1)$$

$$BiONO_3 + Br^- \rightarrow BiOBr + NO_3^- \quad (2)$$

$$8BiOBr + O_2 \rightarrow 2Bi_4O_5Br_2 + 2Br_2\uparrow \quad (3)$$

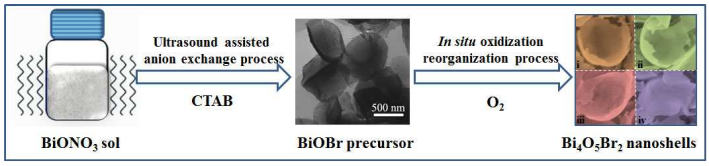

Fig.3 *Schematic illustration of the growth process of ultrathin layered and hollow $Bi_4O_5Br_2$ nanoshells.*

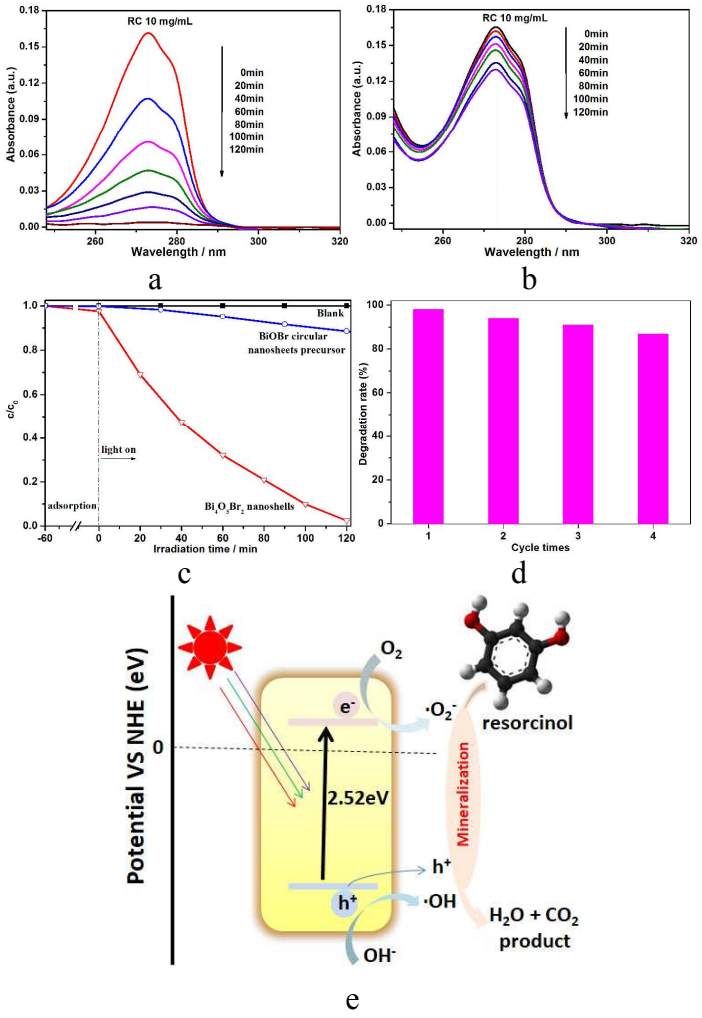

Fig. 4 *The test of photocatalytic degradation activities.*
a Temporal UV-vis absorption spectral changes of RC over $Bi_4O_5Br_2$ nanoshells under visible lighting
b Temporal UV-vis absorption spectral changes of RC over circular sheet-like BiOBr precursor under visible lighting
c The photocatalytic degradation efficiency of RC with the presence of $Bi_4O_5Br_2$ nanoshells and BiOBr nanosheets
d Cycling tests for the photocatalytic degradation rate of RC over $Bi_4O_5Br_2$ nanoshells
e The suggested photocatalytic degradation mechanism of RC over $Bi_4O_5Br_2$ nanoshells

Resorcinol (RC) is a typical colorless and refractory contaminant, of which molecular structure is depicted in Fig. 4e. In this system, the photocatalytic degradation experiments were conducted using RC as a molecular probe under visible light irradiation. As given in Fig. 4a, the

characteristic absorbance of RC at 273 nm declines obviously with the irradiation time over as-prepared 3D multilayered and mesoporous $Bi_4O_5Br_2$ nanoshells. The UV-vis absorption peak of RC solution nearly vanishes after 120 min lighting. For comparison, the removal performance of RC on the same amount of the BiOBr precursor nanosheets was also carried out, as shown in Fig. 4b, one can see that the UV-vis absorption spectra of RC solution is diminished very slowly. Fig. 4c displays the photodegradation efficiency as a function of the irradiation time. It can be found that the direct photolysis of RC could almost be neglected in the blank experiment without photocatalyst. While the degradation percentage of RC over the multilayered and mesoporous $Bi_4O_5Br_2$ nanoshells is about 98.2% after 120 min light irradiation (red line), which is about ten times higher than that of 2D BiOBr nanosheets (*ca.* 9.8%, blue line). In addition, in order to test the stability of the as-obtained $Bi_4O_5Br_2$ nanoshells, the sample was collected after a RC photodegradation experiment. As shown in Fig. 4d, the degradation efficiency of RC is still maintained nearly 90% after four cycles, which indicates that the $Bi_4O_5Br_2$ has good chemical stability during the photocatalysis process. It is a fact that the as-prepared 3D $Bi_4O_5Br_2$ nanoshells exhibit the superior photocatalytic behavior, owing to not only the crystal and band structure, but also the ultrathin layered and shell/hollow feature. Especially, the shell nature is related to a more efficient light-harvesting due to multiple light reflections within the void space; Meanwhile, the ultrathin layered structure is offered to a shorter diffusion length of charge carriers, promoting the separation of the electron-hole pairs and inhibiting the recombination of charge carriers. And then the remarkable photocatalytic activity over the as-fabricated $Bi_4O_5Br_2$ nanoshells is displayed via the primary active species (h^+, •OH radicals and/or $O^{\bullet-}$ anion) oxidized the organics into the small inorganic molecules based on the $Bi_4O_5Br_2$ nanoparticles [14, 18, 21, 22], thus the suggested photocatalytic degradation mechanism of RC over $Bi_4O_5Br_2$ nanoshells might be illustrated in Fig. 4e.

4. Conclusion: In conclusion, novel 3D ultrathin layered $Bi_4O_5Br_2$ nanoshells have been fabricated by two-step process including precipitation reaction in the solution and subsequent calcination in air condition. The unique nanostructures were characterized in detail. The possible formation mechanism was introduced to be the ultrasound assisted anion exchange process and subsequent *in situ* oxidization reorganization process. Additionally, due to the 3D ultrathin layered and mesoporous nanostructures, the photocatalytic performance in the degradation of RC over $Bi_4O_5Br_2$ nanoshells displayed superior efficiency over BiOBr nanosheets as well as other reported $Bi_4O_5Br_2$ nanoarchitectures. Moreover, the $Bi_4O_5Br_2$ nanoshells exhibit good chemical stability and excellent photocatalytic properties during circulatory experiments. It is expected that 3D $Bi_4O_5Br_2$ nanoshells would be advantageous to the practical application in photodegradation of organic pollutants for wastewater purification.

5. Acknowledgments: This work was supported by the Program of Study Abroad for Excellent Young Scholar of Anhui Province (gxfxZD2016221), the Key Projects of Support Program for Outstanding Young Talents of Anhui Province (gxyqZD2016151), the Natural Science Foundation of Anhui Province (1808085MB40), the Natural Science Foundation of Anhui Province Educational Committee (KJ2014ZD08, KJ2015A145), and the Special Foundation for Scientists of Hefei University (15CR06).

6. References

[1] Kudo A., Miseki Y.: 'Heterogeneous photocatalyst materials for water splitting', *Chem. Soc. Rev.*, 2009, **38**, pp. 253-278

[2] Yan J.Q., Wu G.J., Guan N.J., Li L.D.: 'Nb_2O_5/TiO_2 heterojunctions: synthesis strategy and photocatalytic activity', *Appl. Cata.B. Envir.*, 2014, **152-153**, pp. 280-288

[3] Jiang Z.F., Zhu C.Z., Wan W.M., Qian K., Xie J.M.: 'Constructing graphite-like carbon nitride modified hierarchical yolk-shell TiO_2 sphere for water pollution treatment and hydrogen production', *J. Mater. Chem.A.*, 2016, **4**, pp. 1806-1818

[4] Zou Z.G., Ye J.H., Sayama K., Arakawa H.: 'Direct splitting of water under visible light irradiation with an oxide semiconductor photocatalyst', *Nature.*, 2001, **414**, pp. 625-627

[5] Chen X.B., Shen S.H., Guo L.J., Mao S.S.: 'Semiconductor-based photocatalytic hydrogen generation', *Chem. Rev.*, 2010, **110**, pp. 6503-6570

[6] Yu J.G., Low J.X., Xiao W., Zhou P., Jaroniec M.: 'Enhanced photocatalytic CO_2-reduction activity of anatase TiO_2 by co-exposed {001} and {101} facets', *J. Am. Chem. Soc.*, 2014, **136**, pp. 8839-8842

[7] Kubacka A., Fernandez-Garcia M., Colon G.: 'Advanced nanoarchitectures for solar photocatalytic applications', *Chem. Rev.*, 2012, **112**, pp. 1555-1614

[8] Cho I.S., Chen Z.B., Forman A.J., Kim D.R., Rao P.M., Jaramillo T.F., Zheng X.L.: 'Branched TiO_2 nanorods for photoelectrochemical hydrogen production', *Nano. Lett.*, 2011, **11**, pp. 4978-4984

[9] Sun Y.F., Sun Z.H., Gao S., Cheng H., Liu Q.H., Piao J.Y., Yao T., Wu C.Z., Hu S.L., Wei S.Q., Xie Y.: 'Fabrication of flexible and freestanding zinc chalcogenide single layers', *Nat. Commun.*, 2012, **3**, pp. 1057-1063

[10] Sun Y.F., Cheng H., Gao S., Sun Z.H., Liu Q.H., Liu Q., Lei F.C., Yao T., He J.F., Wei S.Q., Xie Y.: 'Freestanding tin disulfide single-layers realizing efficient visible-light water splitting', *Angew. Chem. Int. Ed.*, 2012, **51**, pp. 1-6

[11] Sun Y.F., Gao S., Xie Y.: 'Atomically-thick two-dimensional crystals:electronic structure regulation and energy device construction', *Chem. Soc. Rev.*, 2014, **43**, pp. 530-646

[12] Huang X., Tan C.L., Yin Z.Y., Zhang H.: '25th anniversary article: hybrid nanostructures based on two-dimensional nanomaterials', *Adv. Mater.*, 2014, **26**, pp. 2185-2240

[13] Sun Y.F., Gao S., Lei F.C., Xiao C., Xie Y.: 'Ultrathin two-dimensional inorganic materials: new opportunities for solid state nanochemistry', *Acc. Chem. Res.*, 2015, **48**, pp. 3-12

[14] Di J., Xia J.X., Ji M.X., Yin S., Li H.P., Xu H., Zhang Q., Li H.: 'Controllable synthesis of $Bi_4O_5Br_2$ ultrathin nanosheets for photocatalytic removal of ciprofloxacin and mechanism insight', *J. Mater. Chem. A.*, 2015, **3**, pp. 15108-15118

[15] Li H., Shang J., Ai Z.H., Zhang L.Z.: 'Efficient visible light nitrogen fixation with BiOBr nanosheets of oxygen vacancies on the exposed {001} facets', *J. Am. Chem. Soc.*, 2015, **137**, pp. 6393-6399

[16] Yin H.B., Chen X.F., Hou R.J., Zhu H.J., Li S.Q., Huo Y.N., Li H.X.: 'Ag/BiOBr film in rotating disk reactor containing long afterglow phosphor for round-the-clock photocatalysis', *ACS. Appl. Mater. Inter.*, 2015, **7**, pp. 20076-20082

[17] Deng C.H., Guan H.M.: 'Fabrication of hollow inorganic fullerene-like BiOBr eggshells with highly efficient visible light photocatalytic activity', *Mater. Lett.*, 2013, **107**, pp. 119-122

[18] Zheng C.X., He G.P., Xiao X., Lu M.L., Zhong H., Zuo X.X., Nan J.M.: 'Selective photocatalytic oxidation of benzyl alcohol intobenzaldehyde with high selectivity and conversion ratio over $Bi_4O_5Br_2$ nanoflakes under blue LED irradiation', *Appl. Cata.B. Environ.* 2017, **205**, pp. 201-210

[19] Mao D.J., Ding S.S., Meng L.J., Dai Y.X., Sun C., Yang S.G., He H.: 'One-pot microemulsion-mediated synthesis of Bi-rich $Bi_4O_5Br_2$ with controllable morphologies and excellent visible-light photo-catalytic removal of pollutants', *Appl. Cata.B. Environ.* 2017, **207**, pp. 153-165

[20] Li R., Xie F.X., Liu J.X., Wang Y.W., Wang Y.F., Zhang X.C., Fan C.M.: 'Synthesis of $Bi_4O_5Br_2$ from reorganization of BiOBr and its excellent visible light photocatalytic activity', *Dalton Trans.*, 2016, **45**, pp. 9182-9186
[21] Mao X.M., Xie F.X., Li M.: 'Facile hydrolysis synthesis of novel $Bi_4O_5Br_2$ photocatalyst with enhanced visible light photocatalytic activity for the degradation of resorcinol', *Mater. Lett.*, 2016, **166**, pp. 296-299
[22] Xia J.X., Ge Y.P., Di J., Xu L., Yin S., Chen Z.G., Liu P.J., Li H.M.: 'Ionic liquid-assisted strategy for bismuth-rich bismuth oxybromides nanosheets with superior visible light-driven photocatalytic removal of bisphenol-A', *J. Coll. Inter. Sci.*, 2016, **473**, pp. 112-119
[23] Ye L.Q., Jin X.L., Liu C., Ding C.H., Xie H.Q., Chu K.H., Wong P.K.: 'Thickness-ultrathin and bismuth-rich strategies for BiOBr to enhance photoreduction of CO_2 into solar fuels', *Appl. Cata B: Environ.*, 2016, **187**, pp. 281-290
[24] Bai Y., Ye L.Q., Chen T., Wang P.Q., Wang L., Shi X., Wong P.K.: 'Synthesis of hierarchical bismuth-rich $Bi_4O_5Br_xI_{2-x}$ solid solutions forenhanced photocatalytic activities of CO_2 conversion and Cr(VI) reduction under visible light', *Appl. Cata.B. Environ.* 2017, **203**, pp. 633-640
[25] Zhang X., Ai Z.H., Jia F.L., Zhang L.Z.: 'Generalized one-pot synthesis, characterization and photocatalytic activity of hierarchical BiOX (X = Cl, Br, I) nanoplates microspheres', *J. Phys. Chem. C.*, 2008, **112**, pp. 747-753
[26] Jin X.L., Ye L.Q., Xie H.Q., Chen G.: 'Bismuth-rich bismuth oxyhalides for environmental and energy photocatalysis', *Coor. Chem. Rev.*, 2017, **349**, pp. 84-101
[27] Kudo A., Omori K., Kato H.: 'A novel aqueous process for preparation of crystal form-controlled and highly crystalline $BiVO_4$ powder from layered vanadates at room temperature and its photocatalytic and photophysical properties', *J. Am. Chem. Soc.*, 1999, **121**, pp. 11459-11467
[28] He R., Qian X.F., Yin J., Zhu Z.K.: 'Preparation of Bi_2S_3 nanowhiskers and their morphologies', *J. Crystal Growth*, 2003, **252**, pp. 505-510